Minimization of Cavity Size Ensures Protein Stability and Folding: Structures of Phe46-Replaced Bovine Pancreatic RNase A[†,‡]

Tetsuya Kadonosono,[§] Eri Chatani,*[,§] Rikimaru Hayashi,[§] Hideaki Moriyama,[||] and Tatzuo Ueki[⊥]

Division of Applied Life Sciences, Graduate School of Agriculture, Kyoto University, Sakyo, Kyoto 606-8502, Japan, Chemistry and Biotechnology Center, University of Nebraska-Lincoln, Lincoln, Nebraska 68588-0403 USA, and Japan Synchrotron Radiation Research Institute (JASRI), 1-1 Kouto, Mikazuki, Sayo, Hyogo 679-5198, Japan

Received March 28, 2003; Revised Manuscript Received June 21, 2003

ABSTRACT: The Phe46 residue, located in the hydrophobic core of RNase A, was replaced with other hydrophobic residues, leucine, valine, or alanine, and their X-ray crystallographic structures were determined up to 1.50−1.80 Å resolution in an attempt to examine the relationship between structural changes and conformational stability or folding kinetics. The backbone structure of F46L, F46V, and F46A was indistinguishable from that of the wild-type enzyme, retaining the correct active site structure. However, one water molecule was included in the hydrophobic core of F46A, forming two hydrogen bonds with the backbone peptide chain. The side chain of Met29 in F46V and F46A adopted two different conformations in an equal occupancy. A trapped water molecule and two conformations of Met29 represent changes that minimize the cavity volume. Nevertheless, the replacement of Phe46 with the above residues resulted in a marked decrease in both thermal stability and folding reaction. Thus, Phe46 ensures the thermal stability and the rapid and correct folding of RNase A by the role it plays in forming a highly packed, hydrophobic core.

To explore the factors involved in the rapid and correct folding of proteins, the folding and unfolding processes of bovine pancreatic ribonuclease A (RNase A) [EC 3.1.27.5] (*1*, *2*) have been extensively studied by NMR, FTIR, and other spectroscopic methods (*3*−*8*) as a typical model protein, because this protein is a stable and small monomeric protein composed of 124 amino acids and because it has been established that its three-dimensional structure is fully defined by its amino acid sequence (*9*).

In the folding of RNase A, a nativelike hydrophobic core is formed in the early folding step: The residues involving a hydrophobic collapse or a chain-folding initiation site (CFIS) (the sequence of 106−118 in RNase A) is composed of some ordered structure and forms a core during the correct folding (*10*−*18*). Such a hydrophobic core is also involved in the initial folding processes of other proteins. For an example, the hydrophobic core of α-lactalbumin forms a nativelike structure which stabilizes the molten globular state (*19*) and accelerates the overall refolding reaction (*20*).

A phenylalanine residue at position 46 (Phe46) of RNase A is a key residue in the formation of the hydrophobic core (*21*) and is conserved in seven homologues (bovine seminal ribonuclease, onconase, RNase 1, RNase 2, RNase 3, RNase 4, and angiogenin) (*2*). It is a member of the second *β*-sheet and is completely buried inside the RNase A molecule and is not in contact with solvent waters. It is located in close proximity to the 106−118 CFIS, facing Met29 and Met30, both of which are also highly conserved in the homologues. In a previous study of temperature- and pressure-induced unfolding of wild-type, F46V, F46E, and F46K mutant RNase A (*21*), we concluded that Phe46 is an essential residue in RNase A folding. This conclusion is in good agreement with statistical analyses of the common CFIS sequences among various globular proteins (*22*).

In this study, the thermal unfolding of S−S intact RNase A and the S−S oxidative refolding of RNase A from the fully reduced and unfolded state were examined for the wild-type and mutant (F46L, F46V, and F46A) RNase A, in which Phe46 was genetically replaced by leucine, valine, or alanine. The X-ray crystallographic structures of three mutant RNase A were determined at 1.50−1.80 Å, and structural changes and the cavity formed were correlated with changes in activity, conformational stability, and folding reactions.

MATERIALS AND METHODS

Materials. A DNA plasmid that expresses mutant RNase A was obtained by the method described by delCardayre et al. (*15*, *23*), with minor modifications (*24*). *Escherichia coli* strain BL21(DE3) (*F*$^-$ *ompT hsdS*$_B$(r_B-m_B-) *gal dcm* (DE3)) was purchased from Novagen (Milwaukee, USA). Oligonucleotides were synthesized by Japan Bioservice (Saitama, Japan). The Quickchange Site-Directed Mutagenesis kit was obtained from Stratagene Cloning Systems (California,

[†] This work was supported, in part, by a grant from Japan Space Forum for H.M.

[‡] Structural data: Coordinates have been deposited with Protein Data Bank as 1IZP, 1IZQ, and 1IZR for F46L, F46V, and F46A mutant RNase A, respectively.

* To whom correspondence should be addressed. Division of Applied Life Sciences, Graduate School of Agriculture, Kyoto University, Sakyo, Kyoto 606-8502, Japan. Phone: +81−75−753−6110. Fax: +81−75−753−6128. E-mail: sakurai@kais.kyoto-u.ac.jp.

[§] Kyoto University.

[||] University of Nebraska−Lincoln.

[⊥] JASRI.

10.1021/bi034499w CCC: $25.00
Published on Web 08/20/2003

USA), and the ABI Prism Big Dye Terminator Cycle Sequencing Ready Reaction DNA Sequencing kit was from Perkin-Elmer (California, USA). The IPTG and DTT used for the *E. coli* expression system were from Nacalai Tesque (Kyoto, Japan). C>p[1] was purchased from Seikagaku Kogyo (Tokyo, Japan).

Mutagenesis. Wild-type and F46V mutant RNase A were produced and purified as previously described (*21*). Mutant plasmids used to express the F46L, F46A, and F46G mutant RNase A were constructed with the Quickchange Site-Directed Mutagenesis kit. The primer sequences for F46L were 5′-G CCA GTT AAC ACA TTG GTC CAC GAG AGT TTG GC-3′ and 5′-GC CAA ACT CTC GTG GAC AAC TGT GTT AAC TGG C-3′, those for F46A 5′−G CCA GTT AAC ACA GCT GTC CAC GAG AGT TTG GC-3′ and 5′-GC CAA ACT CTC GTG GAC AGC TGT GTT AAC TGG C-3′, and those for F46G 5′−G CCA GTT AAC ACA GGT GTC CAC GAG AGT TTG GC-3′ and 5′-GC CAA ACT CTC GTG GAC ACC TGT GTT AAC TGG C-3′. Mutations introduced into the plasmid were confirmed by DNA sequencing using an ABI Prism Applied Biosystems 310 Genetic Analyzer by means of dideoxy terminator sequencing. Each mutated plasmid was introduced into *E. coli* strain BL21(DE3), and ampicillin-resistant, transformed cells were used.

Production and Purification of the Wild-Type and the Phe46 Mutant RNase A. The production and purification of F46L, F46A, and F46G were performed by a method similar to those used for the wild-type and F46V mutant RNase A (*21*).

Steady-State Kinetics of Hydrolytic Activity. The hydrolytic reaction for C>p was determined spectrophotometrically (*25*) in 0.2 M sodium acetate buffer (pH 5.5), containing 20 μg/mL enzyme and 0.1−2 mM C>p at 25.0 °C by recording an increase in A_{296} ($\Delta\epsilon_{296}$ of C>p was taken to be 516.4 M^{-1} cm^{-1}). The parameters, K_m and k_{cat}, were evaluated by the Hanes-Woolf plot.

Carboxymethylation. The rate constant for the overall carboxymethylation reaction between iodoacetate and His12 or His119, k_{CM}, was measured by the inhibition of the hydrolytic activity, as described previously (*24*). Two carboxymethylated derivatives (3-CMHis12-RNase A and 1-CM-His119-RNase A) were determined by mono-S chromatography, and the respective rate constants, $k_{CM-His12}$ and $k_{CM-His119}$, were calculated from the magnitude of the ratio of the two derivatives and k_{CM}.

Thermal Denaturation. Thermal unfolding was monitored by changes in the [θ] value at 222 nm using a Jasco J720 spectropolarimeter (Tokyo, Japan) with a jacket cell with a 1-cm-long optical path. Temperature was increased at a rate of 0.5 °C/min by measuring the temperature inside the cell to ensure the temperature equilibrium. The protein concentration was 5.0 μM in a 10 mM MES buffer containing 0.1 M KCl, pH 6.0.

Folding Reaction. The rate of generation of activity was measured for the folding rate from the reduced and unfolded forms of RNase A in the presence of glutathione, as previously described (*26*) with slight modifications: A 1 mL aliquot of a 1 mg/mL protein solution was mixed with 1 mL of 20 mM Tris-HCl, pH 8.0, containing 7 M Gdn-HCl, 10 mM EDTA, and 3.7 mM DTT, and incubated at 25 °C for 2.5 h. Immediately after the Gdn-HCl was removed by a Sephadex G-25 column (15 × 50 mm) equilibrated with 20 mM Tris-HCl (pH 8.0) containing 1 mM EDTA, the protein was diluted with the elution buffer and mixed with GSH and GSSG to initiate the regeneration reaction. The final concentrations of the protein, GSH, and GSSG were 10 μM, 2 mM, and 0.2 mM, respectively. Regenerated activity toward C>p was measured at various times by incubating at 25 °C.

Crystallization. The protein concentration was adjusted to 24 mg/mL with water and subjected to crystallization by the hanging drop vapor diffusion method according to Schultz et al. (*27*) with minor modifications: A 4 μL drop containing an equal volume of the protein and the reservoir solutions and 0.5 mL of reservoir solution composed of 100 mM sodium acetate, pH 6.0, 1.5 M ammonium sulfate, and 2 M NaCl were incubated at 25 °C for the crystallization.

Data Collection and Refinement of X-ray Crystallography. X-ray diffraction data were collected with an ADSC Quantum 4R CCD detector system at SPring-8 (Hyogo, Japan). Beamlines used were the BL44B2 for F46L and F46V, and the BL12B2 for F46A. During the data collection, the crystals were cooled to 100 K. Diffraction images from the CCD detector system were processed and scaled using the HKL2000 program for F46L and F46V, and the DENZO program for F46A (*28*). Details of the data collection are listed in Table 4. The molecular structure was determined by the molecular replacement method using the CNS program (Ver. 1.0) (*29*). The coordinate of the PDB code 1FS3, stripping of all solvent molecules, was used as a starting model. The geometry of the main chain and side chains was analyzed using the PROCHECK program (*30*). The model was adjusted manually in the O program (*31*). After several cycles of least-squares refinements and manual adjustments were performed, water molecules were added to the model. In analyzing conformational changes due to the mutagenic replacement of Phe46, the structures of the wild-type and mutant RNase A were superimposed with the position of the backbone atoms using the CNS program.

RESULTS

Expression and Purification. Ten milligrams of each of the three mutant RNase A (F46L, F46V, and F46A) were obtained from approximately 5 g (wet weight) of *Escherichia coli* cells which were grown in 1-L culture medium. Each of the purified enzymes migrated as a single-stained band on SDS−PAGE and was used in further experiments. The F46G mutant enzyme did not migrate as a single peak on the mono-S column chromatography of the last purification step, since it does not fold into a single correct conformation.

Hydrolytic Reaction for C>p and the Carboxymethylation Rate. The steady-state kinetic parameters of the wild-type and mutant enzymes were determined from their hydrolytic activity toward C>p and are shown in Table 1. The K_m values of the mutant enzymes were judged to be almost the same as that of wild-type enzyme, while k_{cat} values of the mutant enzymes were slightly lower than that of the wild-type enzyme. This indicates that the replacement of Phe46

[1] Abbreviation: C>p, cytidine-2′,3′-cyclic monophosphate; GSH, reduced glutathione; GSSG, oxidized glutathione; RMS, root-mean-square.

Table 1: Kinetic Parameters for the Hydrolysis of C>p and Carboxymethylation by Iodoacetate

RNase A and the mutant enzyme	hydrolysis of C>p			carboxymethylation		
	K_m (mM)	k_{cat} (s^{-1})	k_{cat}/K_m ($s^{-1}\,mM^{-1}$)	k_{CM} ($10^{-4}\,M^{-1}\,s^{-1}$)	$k_{CM-His12}$[a] ($10^{-4}\,M^{-1}\,s^{-1}$)	$k_{CM-His119}$[a] ($10^{-4}\,M^{-1}\,s^{-1}$)
wild type	0.51 ± 0.01	3.49 ± 0	6.87 ± 0.12	114.8 ± 17.9	97.6 ± 15.2	17.2 ± 2.7
F46L	0.42 ± 0.05	2.59 ± 0.12	6.20 ± 0.39	160.0 ± 0.9	144.0 ± 0.8	16.0 ± 0.1
F46V	0.64 ± 0.08	1.61 ± 0.10	2.55 ± 0.16	182.5 ± 10.3	160.6 ± 9.1	21.9 ± 1.2
F46A	0.41 ± 0.02	1.07 ± 0.04	2.59 ± 0.11	90.4 ± 1.3	80.5 ± 1.2	9.9 ± 0.1

[a] Calculated by overall carboxymethylation rate (k_{CM}) and the product ratio of CM-His12 and CM-His119 RNase A.

Table 2: Thermodynamic Parameters for the Thermal Unfolding of Wild-Type and Phe46 Mutant RNase A

RNase A and the mutant enzyme	T_m (K)	ΔH_m (kJ/mol)	ΔS_m (kJ/mol K)	ΔG_{298K} (kJ/mol)	$\Delta\Delta G_{298K}$[a] (kJ/mol)
wild type	332.8	467.2 ± 64.7	1.40	38.9	0
F46L	321.7	410.4 ± 22.6	1.28	25.5	−13.4
F46V	320.7	341.5 ± 19.7	1.06	19.8	−19.0
F46A	310.4	341.2 ± 8.3	1.10	12.3	−26.6

[a] $\Delta\Delta G_{298K} = \Delta G_{298K}$ (mutant) − ΔG_{298K} (wild type).

with leucine, valine, or alanine residue disturbs the catalytic center in some manner, but seems to have no effect on the substrate binding site. Such a small decrease in k_{cat} values, however, would be due to a very slight deviation of His12 and/or His119, as seen in the replacement of Phe120 for tryptophan, alanine, or glycine residues (*32*). A small positional distortion in the two histidines is also supported by only a slight change in the rate of carboxymethylation of His12 and His119, $k_{CM-His12}$ and $k_{CM-His119}$, respectively (Table 1).

Thermal Denaturation. The heat-induced denaturation of mutant enzymes as well as the wild-type enzyme followed two-state transition kinetics with good fitting to eq 1, in which the change in heat capacity (ΔC_p) was fixed at 5.3 kJ/mol (*33*):

$$[\theta] = \frac{([\theta]_n - aT) - ([\theta]_d - bT)}{1 + e^{-[[\Delta H_m(1 - T/T_m) - \Delta C_p\{(T_m - T) + T\ln(T/T_m)\}]/RT]}} + ([\theta]_d - bT) \quad (1)$$

where $[\theta]_n$ and $[\theta]_d$ are $[\theta]$ of the native and denatured states, respectively, and ΔH_m, the enthalpy change of unfolding at T_m. *a* and *b* are factors to correct the baseline slope caused by the temperature-dependent change in $[\theta]$. The entropy changes at T_m, ΔS_m, and the free energy change at 25 °C, ΔG_{298K}, upon protein unfolding were calculated from eqs 2 and 3,

$$\Delta S_m = \Delta H_m/T_m \quad (2)$$

$$\Delta G_{298K} = \Delta H_m(1 - 298/T_m) - \Delta C_p\{(T_m - 298) + 298\ln(298/T_m)\} \quad (3)$$

ΔG_{298K} and ΔH_m values, as well as the T_m value of the wild-type enzyme, were decreased in F46L, F46V, and F46A RNase A, as shown in Table 2. This indicates that the replacement of Phe46 with leucine, valine, or alanine residues caused the destabilization of RNase A. The contribution of Phe46 to the conformational stability of the protein is in good agreement with the previous findings, in which thermal stability of F46V, F46E, and F46K were measured by fourth derivatives of UV absorption spectroscopy (*21*).

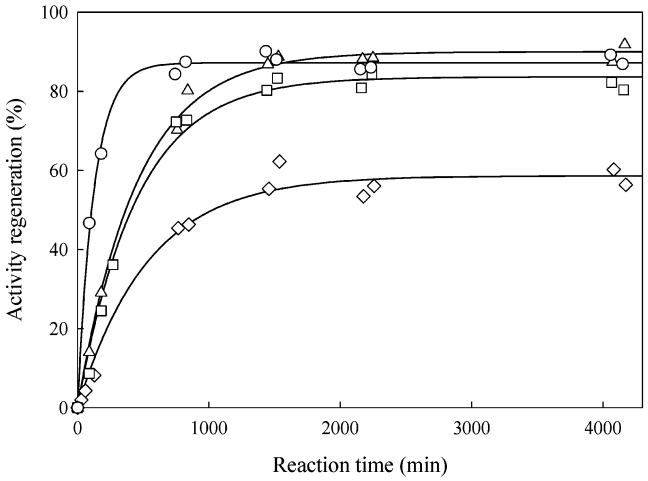

FIGURE 1: Rate of activity regeneration for wild-type (○), F46L (□), F46V (△), and F46A (◇) RNase A from reduced and unfolded states in the presence of glutathione.

Changes in the Folding Rate by the Replacement of Phe46. Being different from the oxidative refolding in the absence of GSH/GSSG, which proceeds via an initial lag phase (*34*, *35*), the regeneration of the RNase A activity in the presence of excess glutathione proceeded with no detectable lag phase (Figure 1). Therefore, the folded (F) and unfolded (U) states were taken to be in equilibrium with the equilibrium constant of *K* as in eqs 4 and 5.

$$U \underset{k_u}{\overset{k_f}{\rightleftharpoons}} F \quad (4)$$

$$K = k_f/k_u \quad (5)$$

The refolding rate is written as eq 6.

$$df/dt = k_f\{1 - e^{-(k_f + k_u)t}\}/(k_f + k_u) \quad (6)$$

where k_f and k_u are the rate constant for folding and unfolding, respectively.

Proline isomerization during the refolding process of RNase A (*7*, *36*) may be observed with the mutant RNase A used in this paper by means of rapid reaction methods.

When the folding and unfolding rate constants of wild-type and mutant enzymes are described as $k_{f,wt}$, $k_{f,mu}$, $k_{u,wt}$, and $k_{u,mu}$, respectively, the differences in the activation free energy between wild-type and mutant enzymes upon folding and unfolding, $\Delta\Delta G_f^{\ddagger}$ and $\Delta\Delta G_u^{\ddagger}$, respectively, can be described by eqs 7 and 8,

$$\Delta\Delta G_f^{\ddagger} = -RT\ln(k_{f,mu}/k_{f,wt}) \quad (7)$$

Table 3: Rate Constants for Folding (k_f) and Unfolding (k_u), Equilibrium Constant (K) between Folded and Unfolded States, Free Energy of Activation for Folding ($\Delta\Delta G_f^{\ddagger}$) and Unfolding ($\Delta\Delta G_u^{\ddagger}$) Reactions, and the Free Energy of Folding ($\Delta\Delta G_K$)

RNase A and the mutant enzyme	k_f[a] (10^{-4}min^{-1})	k_u[a] (10^{-4}min^{-1})	K (k_f/k_u)	$\Delta\Delta G_f^{\ddagger}$[b] (kJ/mol)	$\Delta\Delta G_u^{\ddagger}$[b] (kJ/mol)	$\Delta\Delta G_K$[b] (kJ/mol)	relative activity regeneration (%)
wild type	69.2 ± 3.8	10.2 ± 0.8	6.81	0	0	0	100[c]
F46L	18.5 ± 1.2	3.6 ± 0.5	5.10	3.27	2.55	0.72	96
F46V	19.9 ± 1.0	2.2 ± 0.3	9.00	3.09	3.78	−0.69	103
F46A	10.9 ± 1.2	7.7 ±1.2	1.42	4.58	1.98	3.88	67

[a] Measured by time-dependent activity regeneration in the oxidative refolding reaction at 298 K. See also eq 6. [b] $\Delta\Delta G = \Delta G$ of mutant enzyme − ΔG of wild-type enzyme. [c] Reduced and denatured wild-type RNase A regenerated 87.2% activity in the present conditions.

Table 4: Crystal Properties, Data Collection and Processing, and Refinement of Mutant RNase A

	F46L	F46V	F46A
	Crystal Properties		
space group	$P3_221$	$P3_221$	$P3_221$
a (Å)	63.98	64.12	64.24
c (Å)	63.48	63.38	63.06
	Data Collection and Processing		
X-ray	SPring-8 BL44B2	SPring-8 BL44B2	SPring-8 BL12B2
wavelength (Å)	0.70	0.70	1.00
detector	ADSC Quantum 4R CCD	ADSC Quantum 4R CCD	ADSC Quantum 4R CCD
temp (K)	100	100	100
$\Delta\phi$ (degrees)	1.0	0.5	1.0
max resolution (Å)	1.50	1.50	1.50
process	HKL2000	HKL2000	DENZO
no. of unique reflection	24356	23659	24207
completeness (%)	99.2	96.3	98.8
R_{merge} (%)	0.05	0.08	0.08
	Refinement		
max resolution (Å)	1.50	1.80[a]	1.50
R-factor	0.20	0.20	0.20
R_{free}	0.23	0.24	0.23
RMS deviation of			
(bond distance) (Å)	0.004	0.004	0.004
(bond angle) (degree)	1.2	1.2	1.3

[a] X-ray diffraction images of F46V were collected at maximum resolution of 1.5 Å, but in the structural refinement, the 1.8−1.5 Å diffraction data were cut off for the better refinement statistics.

$$\Delta\Delta G_u^{\ddagger} = -RT \ln(k_{u,mu}/k_{u,wt}) \quad (8)$$

The difference in free energy between folded and unfolded states of the wild-type and mutant enzymes, $\Delta\Delta G_K$, is described as eq 9, when the free energy of wild-type and mutant enzymes are assumed to be K_{wt} and K_{mu}, respectively,

$$\Delta\Delta G_K = -RT \ln(K_{mu}/K_{wt}) \quad (9)$$

As shown in Table 3, the folding rate (k_f) was decreased, with an accompanying increase in the free energy of activation ($\Delta\Delta G_f^{\ddagger}$) by the replacement of Phe46 with leucine, valine, or alanine residues. The unfolding rate (k_u) was also decreased with an increase in the free energy of activation ($\Delta\Delta G_u^{\ddagger}$) by the replacement. The equilibrium constant (K) consistently showed a tendency toward the folded state, regardless of the replacement of Phe46 with leucine, valine, or alanine. In the case of F46A, the accelerated unfolding reaction (k_u) is barely overcome by the moderate folding reaction (k_f) to form the least stable conformation. The unfolding reaction of F46G may be faster than the folding reaction so that a single and stable native conformation is not assumed.

Crystallization, Data Collection, and Structural Refinement. Crystals of F46L, F46V, and F46A mutant RNase A, the sizes of which were about 150 × 150 × 150 μm, were obtained a day after the start of crystallization. The crystal properties and processing of the diffraction data are shown in Table 4. All crystals of the mutant enzymes as well as the wild-type enzyme belonged to the $P3_221$ space group with similar unit cell dimensions. Diffraction data were collected at maximum resolution of 1.50 Å for all mutant enzymes with R_{merge} of 0.05 for F46L, 0.08 for F46V, and 0.08 for F46A. The reflection completeness was 96−99% in all cases. These data made the structural refinement of all mutant enzymes possible.

Refinement of the data are shown in Table 4. The maximum resolution of the refined crystal structures was 1.50 Å for F46L, 1.80 Å for F46V, and 1.50 Å for F46A. In their refined structures, the number of selected water molecules was 206 for F46L, 151 for F46V, and 193 for F46A mutant RNase A. The R-factors of F46L, F46V, and F46A were all 0.20, and the corresponding R_{free} values were 0.23, 0.24, and 0.23, respectively. The RMS values for bond distances and angles were small, indicating that the refinement led to the correct models. All of the $2Fo-Fc$ electron density maps were clear, and examples are shown in Figure 4. The completed coordinates of the mutant RNase A have been deposited in the Protein Data Bank under PDB codes 1IZP (F46L), 1IZQ (F46V) and 1IZR (F46A), respectively. (The coordinate of the wild-type RNase A is deposited as 1FS3, 1RCA, 1RNO, or 1RPH.)

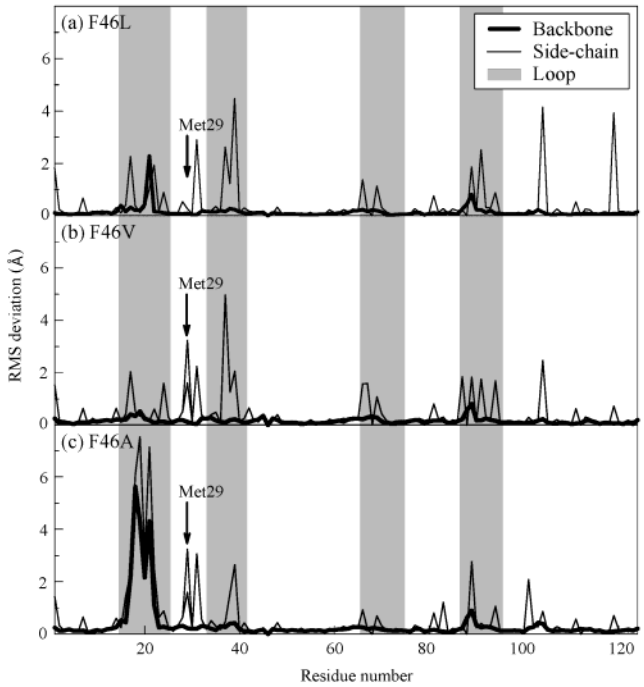

FIGURE 2: Root-mean-square (RMS) deviations of F46L (a), F46V (b), and F46A (c). The structure of each mutant enzyme was superimposed on the wild-type structure (PDB code 1FS3), and the RMS deviation was calculated by using the CNS program (ver. 1.0) (*48*). Bold and thin lines show the backbone and side chains, respectively. Shaded parts represent loop regions of 15−25, 34−41, 65−72, and 87−97. Met29 in F46V and F46A, which fluctuates between two positions, is represented by double peak (see arrows).

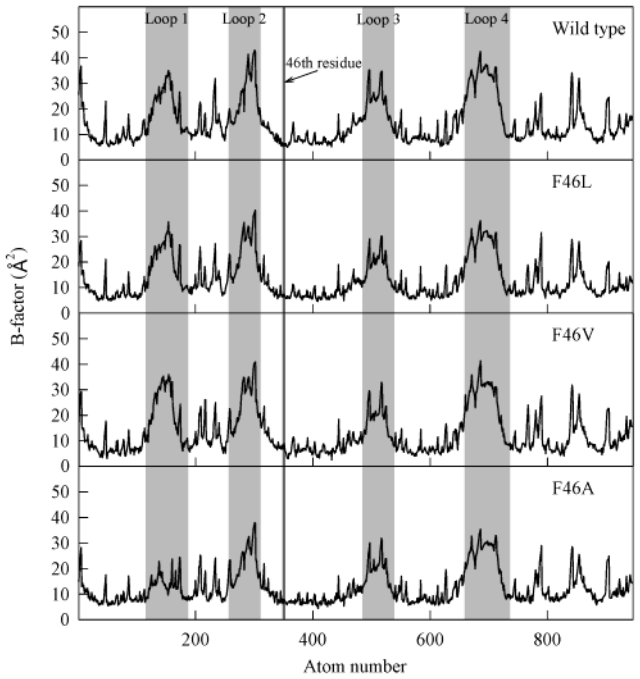

FIGURE 3: B-factors vs atom number of the wild-type, F46L, F46V, and F46A RNase A. Shaded parts represent the loop regions. Only the β-carbons of the side chain in Phe46, Leu46, and Ala46 are indicated.

Backbone structure of mutant RNase A was very similar to that of wild-type enzyme (PDB code 1FS3), except for the loop regions (Figure 2). Deviations in loop regions were judged to be due to their intrinsic flexible features but not due to the effect of the mutation, because the B-factors of the loop regions of the mutant enzymes were as high as those of the wild-type enzyme (Figure 3).

Some side chains except those of the loop regions were slightly deviated by the mutation: Especially Lys1, Lys31, and Lys104 of F46L (Figure 2a), Lys1, Lys31, Lys104 of F46V (Figure 2b), and Lys1, Lys31, Asp83, and Gln101 of F46A (Figure 2c) showed a deviation of more than 1 Å. However, the deviations of Lys1, Lys31, Asp83, Gln101, and Lys104 are not due to the mutation, because the position of these residues was very sensitive to the crystallizing conditions: Deviation of more than 1 Å has been observed on several crystal structures of these residues in wild-type RNase A (the codes 1FS3, 1RCA, 1RNO, and 1RPH of the Protein Data Bank).

His119 adopts either of two positions, A or B, depending on the crystallizing conditions (*37*): It assumed a B position in F46L (PDB code 1IZP), and an A position in the F46V (PDB code 1IZQ) and F46A (PDB code 1IZR) mutant structures. It was judged that His119 is not deviated, because the wild-type structure for the A position (PDB code 1FS3) could be precisely superimposed with F46V and F46A mutant structures of A position, and the wild-type structure of B position (PDB code 1RPH) could be precisely superimposed with the F46L mutant structure of B position.

Met29 of wild-type and F46L mutant RNase A revealed a single 2*Fo*−*Fc* electron density map (Figure 4a,b), but that for the F46V and F46A mutant enzymes revealed two electron density maps with the same density for each (Figure 4c,d). For the two electron density maps, two models are possible: Either the side chain of Met29 takes two different positions in an equal occupancy, or it takes one position, trapping a water molecule in another position. However, when the water molecule was adopted in the density map, the distance between the C_γ atom of Met29 and the oxygen atom of the water was 2 Å or less, too short for noncovalent bond formation. Thus, Met29 of F46V and F46A was judged to take two positions in an equal occupancy: One is directed toward the protein interior with respective RMS deviation values of 3.23 Å for F46V and 3.24 Å for F46A, and the other faces toward the solvent with RMS deviation values of 1.62 Å for F46V and 1.59 Å for F46A.

A globular electron dense spot was found around the alanine residue at position 46 in F46A (shown by an arrow in Figure 4d). This was confirmed by the omit map as well as 2*Fo*−*Fc* electron density map. The B-factor of this electron dense spot was 18.3 Å^2, the size of which could be regarded as an oxygen atom of a water molecule. Thus, the spot was fitted to a water molecule rather than an ammonium, sodium, or chloride ion, which were present in the crystallization medium. The water molecule trapped around the Ala46 possibly formed two hydrogen bonds with α-carboxyl oxygen in 2.95 Å distance and $N_{\delta 2}$ of Asn44 in 2.85 Å distance.

Cavity Creation Formed by the Mutation of Phe46. The replacement of Phe46 of RNase A with smaller residues, such as leucine, valine, or alanine residues (F46L, F46V, or F46A) led to the very similar overall structure with that of wild-type enzyme, and a cavity was formed around the place where the benzene ring of Phe46 originally existed (Figure 4). The difference in the cavity volume between wild-type and mutant enzymes was 31.6 Å^3 for F46L, 30.9 Å^3 for

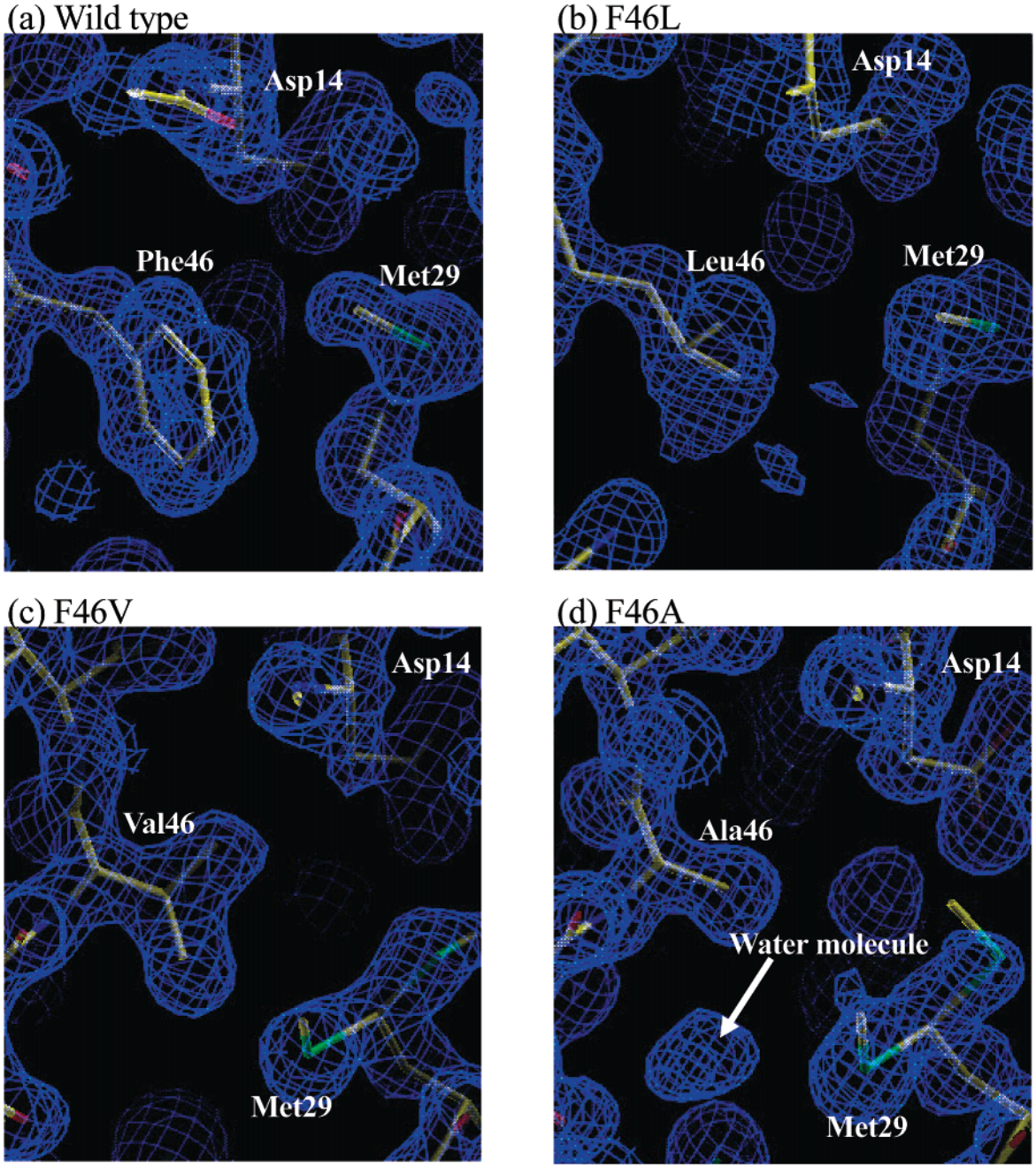

FIGURE 4: Electron density (2*Fo*−*Fc*) maps of (a) wild type, (b) F46L, (c) F46V, and (d) F46A around Phe46 and its replaced residues. Figures are drawn with the O program (*31*), contoured at 1.0 Å. C (yellow), O (red), N (blue), and S (green) atoms are shown. The density of the water molecule (shown by an arrow) is located around Ala46 in F46A. Stick models represent finally refined models.

F46V, and 35.9 Å^3 for F46A (including a water molecule), when calculated using the CASTp program (*38*−*40*) with a 1.4 Å probe radius (Table 5), not to correspond to the volume difference of side chains between phenylalanine and leucine (difference of 11 Å^3), valine (difference of 30 Å^3), or alanine residues (difference of 68 Å^3). Moreover, the difference in the cavity volume between wild-type RNase A and F46V or F46A was smaller than the expected values, 77.70 and 128.32 Å^3, respectively, calculated on the basis of the structural coordinate of the wild-type enzyme with the manual replacement of Phe46 with valine or alanine residues. These smaller cavities are due to the movement of Met29 residues of F46V and F46A and a trapped water molecule in F46A to decrease the cavity volume.

DISCUSSION

The replacement of Phe46 of RNase A with leucine, valine, or alanine residues adversely affected the conformational stability and the folding speed with only a slight effect on the conformation of the active site. The reason a phenylalanine residue must occupy position 46 of RNase A is as follows:

Role of Phe46 in the Conformational Stability of RNase A. The free energy difference upon thermal unfolding between the wild-type enzyme and mutant enzymes (F46L, F46V, and F46A), $\Delta\Delta G_{298K}$ (Table 2), and the increase in cavity volume by the mutation, ΔV_c (Table 5), were correlated in a linear manner with the slope of −636 J/mol/Å^3 and the correlation coefficient of 0.92 (Figure 5). This

Table 5: Difference in Cavity Volume of Wild-Type and Mutant RNase A[a]

RNase A and the mutant enzyme	cavity volume (Å^3) observed	cavity volume (Å^3) expected[c]	difference in van der Waals volume between phenylalanine and its replaced residue (Å^3)
wild type	0	0	0
F46L	31.6	29.05	11
F46V	30.9[b]	77.70	30
F46A	35.9[b]	128.32	68
F46G		162.11	87

[a] Calculated by the CASTp program (*38*−*40*) following the procedure of Connolly (*49*). [b] Average cavity volume of two different conformations caused by the two different occupancies of Met29. [c] Estimated by the manual replacement of Phe46 on the basis of the coordinate of wild-type RNase A.

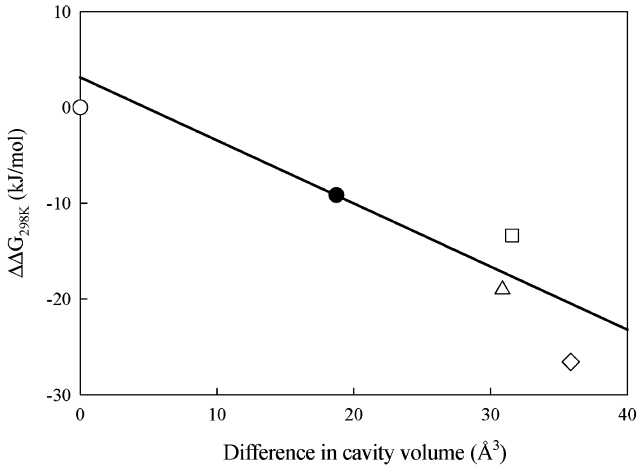

FIGURE 5: Correlation between the difference in thermal unfolding energy ($\Delta\Delta G_{298K}$) and the difference in cavity volume (ΔV_c) of wild-type (○), F46L (□), F46V (△), F46A (◇) RNase A, and V16A RNase T1 (●) (*41*). The energy decrease upon unfolding per 1 Å^3 of the cavity volume is calculated to be 0.636 kJ mol^{-1} Å^{-3} from the slope of a fitted straight line with the correlation coefficient of 0.92.

correlation was also found for the V16A mutant RNase T1 (*41*), when their cavity volumes were recalculated by the CASTp program, resulting in a calculated probe radius of 1.4 Å. This result indicates that an increase in the cavity volume of the hydrophobic core decreases the overall structural stability of the protein. Thus, the tightly packed hydrophobic core by Phe46 ensures the conformational stability of RNase A.

The decrease in ΔG_{298K} accompanying the increase in cavity volume was 636 J mol^{-1} Å^{-3} in the case of RNase A and its Phe46 mutant enzymes (Figure 5), but is only 100 J mol^{-1} Å^{-3} in the case of the T4 lysozyme and its Leu46, Leu99, Leu118, Leu121, Leu133, and Phe153 mutant enzymes (*42*). This great contribution of Phe46 to ensure conformational stability would be due to the tight packing of the hydrophobic core, because the number of atoms located within 6 Å from the C_α atom of Phe46 of RNase A and that of Val16 of RNase T1 are 58 and 57, respectively, but that of Leu46, Leu99, Leu118, Leu121, Leu133, and Phe153 of the T4 lysozyme and that of Ile96 of barnase (*43*) are, at most, 48. As the tightly packed hydrophobic core restricts the movement of residues, the rearrangement of the core to compensate the decrease in stability is limited. Moreover, disulfide bonds would also restrict the movement. The number of disulfide bonds of RNase A and RNase T1 are 4 and 2, respectively, but that of both T4 lysozyme and barnase are 0. Therefore, the movement of residues of RNase A and RNase T1 are more restricted by disulfide bonds than that of T4 lysozyme and barnase. Such a great contribution of Phe46 is not the result of the interaction of π-electrons of Phe46 and cation of Arg33, which is the only one cationic site located within 6 Å of the center of Phe46 ring, is based on the following two reasons. First, π-cation interactions commonly occur within an α-helix, but Phe46 forms a β-sheet (*44*). Second, the nitrogen atom of the NH−C_ζ bond of the arginine residue is not in parallel or in a T-shaped position against the face of benzene ring, necessary conditions for the guanidido group to participate in a π-cation interaction (*44*).

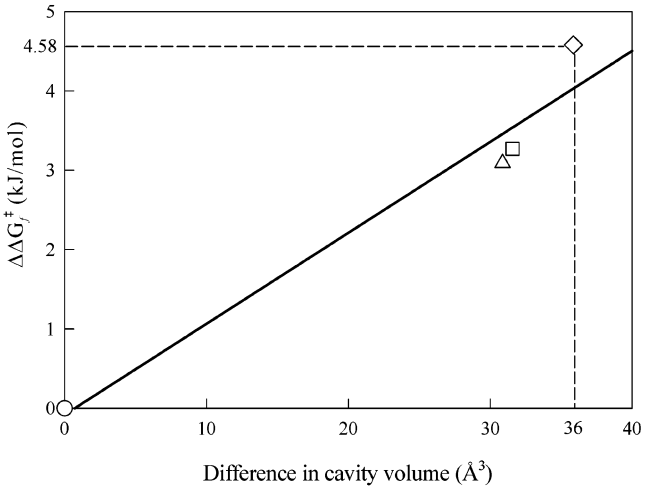

FIGURE 6: Correlation between the difference in activation energy of folding ($\Delta\Delta G_f^{\ddagger}$) and the difference in the cavity volume (ΔV_c) of wild-type (○), F46L (□), F46V (△), F46A (◇) RNase A. The energy increase for folding per 1 Å^3 of cavity volume is calculated to be 0.115 kJ mol^{-1} Å^{-3} from the slope of a fitted line with the correlation coefficient of 0.98.

The water molecule located around Ala46 in F46A can form two hydrogen bonds with an α-carboxyl oxygen and $N_{\delta 2}$ atoms of Asn44 at a distance of 2.95 Å and 2.85 Å, respectively. According to previous reports (*45*, *46*), a water molecule buried in the hydrophobic core gains approximately 5 kJ/mol by forming one hydrogen bond, although it loses 7.54−10.0 kJ/mol from unfavorable entropy changes and loss of hydrogen bonds to other solvent water molecules. Thus, the energy loss to trap a water molecule in the hydrophobic core of F46A is barely offset by the two hydrogen bonds formed. Thus, a decrease in the cavity results.

Free energy differences between native and unfolded enzymes ($\Delta\Delta G_K$) calculated from eq 9 increased with an increase in the cavity volume, ΔV_c (Tables 3 and 5). This is consistent with the thermal unfolding results (Figure 5).

The Role of Phe46 in the Folding of RNase A. The free energy of activation upon folding ($\Delta\Delta G_f^{\ddagger}$) is increased by an increase in the cavity volume (ΔV_c) (see Figure 6), indicating that the hydrophobic core must be well packed to realize folding. The increase in the free energy of activation is estimated to be 0.115 kJ mol^{-1} Å^{-3} from the slope of the plot shown in Figure 6. Thus, F46A RNase A will not fold to the native state unless one water molecule is trapped. F46G RNase A cannot correctly fold because of its overly large cavity volume (Table 5). Some mutant T4 lysozyme trapped a benzene molecule in their cavities with an increase in T_m

by 3−6 K (*47*). This interesting phenomenon should be tested with F46G mutant RNase A. The limit of the cavity volume and the free energy of activation for the polypeptide to correctly fold are estimated to be approximately 36−162 Å^3 and over 4.58 kJ/mol, respectively. Thus, the folding reaction is ensured by the tight packing of the hydrophobic core with the minimum cavity size.

The free energy of activation for unfolding ($\Delta\Delta G_u^{\ddagger}$) showed no correlation with the cavity volume (see Table 3). This is because $\Delta\Delta G_u^{\ddagger}$ is determined by two terms, $\Delta\Delta G_f^{\ddagger}$ and $\Delta\Delta G_K$ ($\Delta\Delta G_u^{\ddagger} = \Delta\Delta G_f^{\ddagger} - \Delta\Delta G_K$). That is, since both $\Delta\Delta G_f^{\ddagger}$ and $\Delta\Delta G_K$ are increased with an increase in cavity volume (Table 3 and Figure 6), $\Delta\Delta G_u^{\ddagger}$ is determined by the balance of $\Delta\Delta G_f^{\ddagger}$ and $\Delta\Delta G_K$.

Moreover, the clear proportionality between $\Delta\Delta G_f^{\ddagger}$ and the cavity volume, as shown in Figure 6, leads to a further suggestion that $\Delta\Delta G_f^{\ddagger}$ directly reflects the cavity forming reaction. If the folding reaction were to be separated into two steps, one of which being the initial step as forming small ordered several hydrophobic collapses from the randomly disordered structure, and the other of which is a later step containing a nativelike structure, the highest energy barrier for this refolding process would belong to the later step, since a nativelike cavity cannot be formed at such a disordered initial state. Phe46 therefore appears to contribute to the acceleration in the formation of nativelike hydrophobic core structure in the later stage.

CONCLUSION

Phe46 in RNase A ensures conformational stability and correct folding by forming a tightly packed hydrophobic core. When the Phe46 is replaced by other amino acid residues, the cavity of the core could be compensated by moving of Met29 or by trapping a water molecule to decrease the cavity.

ACKNOWLEDGMENT

We thank Drs. Shinichi Adachi, Riken Harima Institute/SPring-8, and Mau-Tsu Tang, Asia and Pacific Council for Science and Technology, at BL44B2 and BL12B2 beamlines, respectively, in SPring-8 for their help in data collection.

REFERENCES

1. Cuchillo, C. M., Vilanova, M., and Nogues, M. V. (1997) in *Ribonucleases: Structures and Functions* (D'Alessio, G., and Riordan, J. F., Eds.) pp 271−300, Academic press, New York.
2. Raines, R. T. (1998) *Chem. Rev. 98*, 1045−1066.
3. Schmid, F. X. (1982) *Eur. J. Biochem. 128*, 77−80.
4. Dodge, R. W., Laity, J. H., Rothwarf, D. M., Shimotakahara, S., and Scheraga, H. A. (1994) *J. Protein Chem. 13*, 409−421.
5. Houry, W. A., Rothwarf, D. M., and Scheraga, H. A. (1995) *Nat. Struct. Biol. 2*, 495−503.
6. Houry, W. A., and Scheraga, H. A. (1996) *Biochemistry 35*, 11734−11746.
7. Sendak, R. A., Rothwarf, D. M., Wedemeyer, W. J., Houry, W. A., and Scheraga, H. A. (1996) *Biochemistry 35*, 12978−12992.
8. Houry, W. A., Rothwarf, D. M., and Scheraga, H. A. (1996) *Biochemistry 35*, 10125−10133.
9. Anfinsen, C. B. (1973) *Science 181*, 223−230.
10. Nemethy, G., and Scheraga, H. A. (1979) *Proc. Natl. Acad. Sci. U.S.A. 76*, 6050−6054.
11. Gutte, B. (1977) *J. Biol. Chem. 252*, 663−670.
12. Haas, E., Montelione, G. T., McWherter, C. A., and Scheraga, H. A. (1987) *Biochemistry 26*, 1672−1683.
13. Morgan, C. J., Miranker, A., and Dobson, C. M. (1998) *Biochemistry 37*, 8473−8480.
14. Beals, J. M., Haas, E., Krausz, S., and Scheraga, H. A. (1991) *Biochemistry 30*, 7680−7692.
15. Dodge, R. W., and Scheraga, H. A. (1996) *Biochemistry 35*, 1548−1559.
16. Coll, M. G., Protasevich, I. I., Torrent, J., Ribo, M., Lobachov, V. M., Makarov, A. A., and Vilanova, M. (1999) *Biochem. Biophys. Res. Commun. 265*, 356−360.
17. Torrent, J., Connelly, J. P., Coll, M. G., Ribo, M., Lange, R., and Vilanova, M. (1999) *Biochemistry 38*, 15952−15961.
18. Torrent, J., Rubens, P., Ribo, M., Heremans, K., and Vilanova, M. (2001) *Protein Sci. 10*, 725−734.
19. Wu, L. C., and Kim, P. S. (1998) *J. Mol. Biol. 280*, 175−182.
20. Villegas, V., Martinez, J. C., Aviles, F. X., and Serrano, L. (1998) *J. Mol. Biol. 283*, 1027−1036.
21. Chatani, E., Nonomura, K., Hayashi, R., Balny, C., and Lange, R. (2002) *Biochemistry 41*, 4567−4574.
22. Poupon, A., and Mornon, J. P. (1999) *FEBS Lett. 452*, 283−289.
23. delCardayre, S. B., Ribo, M., Yokel, E. M., Quirk, D. J., Rutter, W. J., and Raines, R. T. (1995) *Protein Eng. 8*, 261−273.
24. Chatani, E., Tanimizu, N., Ueno, H., and Hayashi, R. (2001) *J. Biochem. 129*, 917−922.
25. Boix, E., Nogues, M. V., Schein, C. H., Benner, S. A., and Cuchillo, C. M. (1994) *J. Biol. Chem. 269*, 2529−2534.
26. Fujii, T., Ueno, H., and Hayashi, R. (2002) *J. Biochem. 131*, 193−200.
27. Schultz, L. W., Hargraves, S. R., Klink, T. A., and Raines, R. T. (1998) *Protein Sci. 7*, 1620−1625.
28. Otwinowski, Z., and Minor, W. (1997) *Methods Enzymol. 276*, 307−326.
29. Brunger, A. T., Adams, P. D., Clore, G. M., Delano, W. L., Gros, P., Grosse-Kunstleve, R. W., Jiang, J.-S., Kuszewski, J., Nilges, N., Pannu, N. S., Read, R. J., Rice, L. M., Simonson, T., and Warren, G. L. (1998) *Acta Crystallogr. D54*, 905−921.
30. Laskowski, R. A., McArthur, M. W., Moss, D. S., and Thorton, J. M. (1993) *J. Appl. Crystallogr. 24*, 282−291.
31. Jones, T. A., Zou, J.-Y., Cowan, S. W., and Kjeldgaard, M. (1991) *Acta Crystallogr. A47*, 110−119.
32. Chatani, E., Hayashi, R., Moriyama, H., and Ueki, T. (2002) *Protein Sci. 11*, 72−81.
33. Makhatadze, G. I., and Privalov, P. L. (1995) *Adv. Protein Chem. 47*, 307.
34. Rothwarf, D. M., Li, Y. J., and Scheraga, H. A. (1998) *Biochemistry 37*, 3767−3776.
35. Fujii, T., Doi, Y., Ueno, H., and Hayashi, R. (2000) *J. Biochem. 127*, 877−881.
36. Cook, K. H., Schmid, F. X., and Baldwin, R. L. (1979) *Proc. Natl. Acad. Sci. U.S.A. 76*, 6157−6161.
37. de Mel, V., Doscher, M., Martin, P., and Edwards, B. (1994) *FEBS Lett. 349*, 155−60.
38. Liang, J., Edelsbrunner, H., and Woodward, C. (1998) *Protein Sci. 7*, 1884−1897.
39. Liang, J., Edelsbrunner, H., Fu, P., Sudhakar, P. V., and Subramaniam, S. (1998) *Proteins 33*, 1−17.
40. Liang, J., Edelsbrunner, H., Fu, P., Sudhakar, P. V., and Subramaniam, S. (1998) *Proteins 33*, 18−29.
41. Vos, S. D., Backmann, J., Prevost, M., Steyaert, J., and Loris, R. (2001) *Biochemistry 40*, 10140−10149.
42. Eriksson, A. E., Baase, W. A., Zhang, X. J., Heinz, D. W., Blaber, M., Baldwin, E. P., and Matthews, B. W. (1992) *Science 255*, 178−183.
43. Serrano, L., Kellis, J. T., Jr., Cann, P., Matouschek, A., and Fersht, A. R. (1992) *J. Mol. Biol. 224*, 783−804.
44. Gallivan, J. P., and Dougherty, D. A. (1999) *Proc. Natl. Acad. Sci. U.S.A. 96*, 9459−9464.
45. Funahashi, J., Takano, K., Yamagata, Y., and Yutani, K. (1999) *Protein Eng. 12*, 841−850.
46. Dunitz, J. D. (1994) *Science 264*, 670.
47. Eriksson, A. E., Baase, W. A., Wozniak, J. A., and Matthews, B. W. (1992) *Nature 355*, 371−373.
48. Brunger, A. T. (1992) X-PLOR Version 3.1 Manual: A System for Crystallography and NMR, Yale University, New Haven, CT.
49. Connolly, M. L. (1993) *J. Mol. Graph. 11*, 139−141.

BI034499W